Presynaptic Monoaminergic Vesicles in Parkinson's Disease and Normal Aging

Kirk A. Frey, MD, PhD,*†‡ Robert A. Koeppe, PhD,* Michael R. Kilbourn, PhD,*
Thierry M. Vander Borght, MD,* Roger L. Albin, MD,† Sid Gilman, MD,† and David E. Kuhl, MD*

We present development and human application of a method for determining the regional cerebral density of the type 2 vesicular monoamine transporter (VMAT2) using positron emission tomography (PET) and [^{11}C]dihydrotetrabenazine (DTBZ). Previous animal studies indicate striatal VMAT2 density is linearly related to the integrity of substantia nigra dopamine neurons and is not subject to drug- or lesion-compensatory regulation. In the present studies, kinetic compartmental modeling was employed to estimate blood–brain [^{11}C]DTBZ transport (K_1) and VMAT2 binding site density (tissue-to-plasma DTBZ distribution volume, *DV*) from the cerebral and plasma DTBZ time courses after intravenous tracer injection. In controls, we found reductions of putamen DTBZ *DV* with advancing age, corresponding to losses of 0.77% per year in specific VMAT2 binding. Parkinson's disease (PD) patients had reduction in specific DTBZ *DV* in the putamen (−61%) and in the caudate nucleus (−43%). There was no overlap of lowest specific putamen DTBZ *DV* between individual elderly controls and PD patients. The present results indicate the suitability of [^{11}C]DTBZ PET for objective quantification of nigrostriatal integrity, including evaluation of PD progression and its possible therapeutic modification.

Frey KA, Koeppe RA, Kilbourn MR, Vander Borght TM, Albin RL, Gilman S, Kuhl DE. Presynaptic monoaminergic vesicles in Parkinson's disease and normal aging. Ann Neurol 1996;40:873–884

Pathological losses of dopaminergic neurons in the ventral midbrain and their striatal terminals are well recognized in idiopathic Parkinson's disease (PD) [1, 2] and in other neurodegenerative extrapyramidal movement disorders such as multiple system atrophy [3] and progressive supranuclear palsy [4]. Despite this knowledge, the pathophysiology of selective nigrostriatal injury, and thus therapies to slow or arrest the progression of PD, are unknown. Effects of environmental toxins [5, 6], genetic predisposition [7], oxidative stress [8, 9], and even differing symptomatic therapies [10, 11] on the development and progression of PD have been proposed. An objective, noninvasive marker of nigrostriatal pathology would be helpful to advance our current understanding of PD and to permit direct testing of these hypotheses.

Several radiotracers have been employed previously to image nigrostriatal terminals and the changes in PD in vivo, including [^{18}F] fluoroDOPA (FDOPA) [12], [^{11}C]nomifensine [13], [^{11}C]WIN 35,428 [14], and [^{123}I]β-CIT [15]. Unfortunately, the processes revealed by these ligands are subject to drug-induced and disease-compensatory regulation, limiting their abilities to quantify accurately PD lesion severity [16]. In the present studies, we introduce the novel ligand [^{11}C]dihydrotetrabenazine ([^{11}C]DTBZ) for in vivo binding estimates of the type 2 vesicular monoamine transporter (VMAT2) in the human brain. Prior studies of this presynaptic monoaminergic binding site in experimental animals indicate that it is not regulated readily by conditions that alter the synthesis, turnover, or release of dopamine [17, 18]. Further, its striatal concentration is highly correlated with the number of intact nigral dopaminergic neurons following graded neurotoxin lesions [19], suggesting that VMAT2 density may be an objective marker of nigrostriatal terminal integrity. The current studies extend our investigations of [^{11}C]DTBZ biodistribution to the human brain with positron emission tomography (PET), including development of a quantitative PET VMAT2 assay, examination of VMAT2 binding in normal aging, and a comparison with PD patients. In an accompanying report, [^{11}C]DTBZ binding to straital VMAT2 in patients with multiple system atrophy or sporadic olivopontocerebellar atrophy is examined [20].

Subjects and Methods

Metabolism and Chromatography of DTBZ

Preclinical studies were conducted with [^{3}H]DTBZ in the rat to detect the presence of radiolabeled metabolites of

From the Departments of *Internal Medicine (Division of Nuclear Medicine) and †Neurology, and ‡Mental Health Research Institute, University of Michigan, Ann Arbor, MI.

Received Feb 1, 1996, and in revised form May 30. Accepted for publication May 31, 1996.

Address correspondence to Dr Frey, The University of Michigan Hospitals, B1G 412/0028 AGH, 1500 East Medical Center Drive, Ann Arbor, MI 48109-0028.

Copyright © 1996 by the American Neurological Association

[^{11}C]DTBZ in blood and tissues and to establish a rapid chromatographic method for assay of authentic DTBZ in plasma. (9-*O*-[$^{3}H_3$]Methoxy)DTBZ (sp act, 82 Ci/mmol) was custom synthesized from the desmethyl precursor and [^{3}H]CH_3I (Amersham Corp, Arlington Heights, IL). Approximately 15 minutes after intravenous injection of 1 mCi [^{3}H]DTBZ in a 225-gm male Sprague–Dawley rat, arterial blood was sampled and the rat was killed by intravenous injection of pentobarbital followed by saturated KCl to produce cardioplegia. Plasma aliquots were analyzed by liquid scintillation spectroscopy both directly and after deproteination by the addition of 3 volumes of absolute ethanol and centrifugation at 10,000 × *g* for 10 min. Samples of brain and liver were homogenized in ethanol (3:1, vol/tissue weight), and aliquots of the total homogenates and postcentrifugation supernatants were assayed to assess recovery. Additional aliquots of the ethanolic tissue and plasma supernatants were concentrated under vacuum and further analyzed by thin-layer chromatography (TLC) on silica gel plates (E. Merck no. 5721, Darmstadt, Germany) with a mobile phase of chloroform/methanol 96:4. Chromatograms were autoradiographed by apposition to x-ray film (SB5, Eastman Kodak, Rochester, NY) at −70°C for 3 days with the use of a fluorographic enhancer (En^{3}hance, Amersham Corp). Labeled species identified in the autoradiograms were scraped from the TLC plates and assayed by liquid scintillation spectroscopy.

Samples of radiolabeled, polar [^{3}H]DTBZ metabolites obtained from TLC of liver were employed in conjunction with authentic [^{3}H]DTBZ to develop a rapid liquid chromatographic procedure for their separation. Samples of DTBZ or labeled metabolites were applied to Whatman Sep-Pak C_{18} chromatography columns (Waters Division, Millipore Corp, Milford, MA) in 1 ml of phosphate-buffered saline (PBS; NaCl 124 mM, KCl 2.7 mM, Na_2HPO_4 7.7 mM, KH_2PO_4 1.5 mM, pH 7.4) and eluted with 9 ml ethanol/PBS mobile phases of varying proportion followed by 5 ml of absolute ethanol. Eluates were assayed in sequential 1-ml fractions by liquid scintillation spectroscopy to determine both elution profile and sample recovery.

Subjects

Six young (age, 26 ± 4 years; range, 22–34 years; 2 females, 4 males), 3 middle-aged (age, 47 ± 4 years; 44–52 years; 3 females), and 6 elderly (age, 64 ± 5 years; range 57–70 years; 1 female, 5 males) normal subjects were studied in comparison with 7 PD patients (age, 67 ± 7 years; range, 57–79 years; 2 females, 5 males). The PD patients each had the cardinal signs of resting tremor, bradykinesia, and rigidity with symptomatic and objectively documented responsiveness to levodopa. The patients ranged in severity between stages I and III on the Hoehn and Yahr scale [21], with symptomatic durations of illness between 3 and 10 years. Normal subjects were receiving no centrally acting medications, whereas the PD patients were receiving levodopa/carbidopa, amantadine, or deprenyl; antiparkinsonian medications were not discontinued prior to [^{11}C]DTBZ imaging. The experimental protocol was approved by The University of Michigan committees on the use of human subjects in research and on the human use of radioisotopes, and written informed consent was obtained prior to all procedures.

[^{11}C]DTBZ Scans

Carbon-11–labeled, racemic (±)-DTBZ was prepared by methylation of the desmethyl precursor as described previously [22, 23]. The specific activity of [^{11}C]DTBZ was determined by high-performance liquid chromatography and ultraviolet absorption spectrometry in conjunction with radioassay in an ionization chamber, and was routinely in the range of 500 to 1,000 Ci/mmol at end-of-synthesis.

Subjects were studied in a Siemens-CTI 921 Exact tomograph, which images a 15.8-cm axial field-of-view and permits reconstruction of 47 contiguous 3.375-mm-thick axial slices in the septa-in scanning configuration. All subjects were studied supine, with eyes and ears unoccluded, resting quietly in a dimly lit room. After the catheterization of a radial artery and contralateral antecubital vein, four porous beads of approximately 1-mm diameter were labeled with 1 μCi [^{11}C]DTBZ and affixed to widely separated locations on the scalp, within the scanned field-of-view. Scans were then initiated with the bolus intravenous injection of approximately 18 mCi [^{11}C]DTBZ containing less than 50 μg of mass. Dynamic PET imaging of the head was performed over 60 minutes according to the following schedule: 4 × 30-second, 3 × 1-minute, 2 × 2.5-minute, 2 × 5-minute, and 4 × 10-minute scan durations. Scans were reconstructed by filtered back projection employing a Hanning filter with cutoff frequency of 0.5 cycles/ray and calculated attenuation correction. Dynamic sequences of scans were next corrected for subject motion during the session on the basis of the fiducial scalp markers. The locations of the beads were identified in a reference frame and all other frames in the time sequence were reoriented (6 degrees of freedom, three translational and three rotational) to bring the fiducials to the same coordinates throughout the entire sequence. Anatomically configured regions of interest corresponding to the midfrontal cortex, caudate nucleus, putamen, thalamus, and cerebellum were applied to the sequence of images in each subject's scan. Regional boundaries were defined on summed [^{11}C]DTBZ activity maps from 0 to 7.5 minutes after injection, and were applied in parallel to the three contiguous axial slices that best represented the body of the thalamus (thalamus and frontal cortex), the striatum (caudate and putamen), and the midcerebellum.

Heparinized arterial blood was collected at 10-second intervals for 2 minutes, followed by additional samples at 2.5, 3, 4, 5, 7.5, 10, 15, 30, 45, and 60 minutes after injection of [^{11}C]DTBZ. After centrifugation, total plasma activity was determined in aliquots with a sodium iodide well counter. Aliquots at 1-minute, 2-minute, 3-minute, and later postinjection times were processed in parallel for determination of radiolabeled metabolites. Plasma (0.5 ml) was added to PBS (0.5 ml) containing approximately 0.05 μCi of authentic [^{3}H]DTBZ, and the sample was applied to a Sep-Pak C_{18} chromatography column. The eluates (1) from initial loading combined with a subsequent wash with 9 ml of PBS/ethanol 65:35; and (2) from a subsequent wash with 5 ml of absolute ethanol were assayed for carbon-11 activity in the well counter. After decay of the carbon-11, aliquots of the two eluates were assayed for tritium content by liquid scintillation spectrometry. The distributions of total carbon-11 and [^{3}H]DTBZ were then employed to calculate the fractions of authentic [^{11}C]DTBZ and carbon-11–labeled metabolites in plasma, as described previously [24].

Parametric Analyses of DTBZ Distribution

Estimates of tracer delivery to brain were derived from the blood–brain barrier rate parameter (K_1) and of VMAT2 binding site density from tissue-to-blood tracer distribution volumes (DVs), each determined from cerebral and metabolite-corrected arterial plasma [^{11}C]DTBZ time–activity curves (see Appendix). In prior studies with reversible binding ligands, the total tissue *DV* has been investigated and established as an estimate of binding site density [25, 26]. The total *DV* parameter has the advantage of favorable precision and stability; however, it contains contributions of nonspecific and free ligand in addition to that of specific binding. We also estimated, as follows, the component of total DTBZ *DV* attributable to specific binding with the use of the frontal cortex as a reference region essentially devoid of VMAT2 binding sites relative to the normal striatum:

$$DV_{specific} = (DV_{total} - DV_{cortex})/DV_{cortex}$$

Our assumption of minimal specific DTBZ binding in the frontal cortex relative to the striatum is supported by (1) in vitro VMAT2 binding results in rodent and human brain that indicate cortical binding levels between 5% and 8% of those in the caudate nucleus and putamen [19, 27]; and (2) relative levels of monoamines in human brain indicating cortical values of less than 1% of the caudata nucleus [28].

Data Analysis and Statistics

Parametric regional determinations of DTBZ K_1 and total *DV* were averaged from left and right hemispheres and assessed with one-way analysis of variance (ANOVA) (within brain region) across young, middle-aged, and elderly normal and PD patient groups. Data from regions demonstrating significant ANOVA were then examined with pairwise Student's *t* tests for difference from the elderly controls. Additional comparisons of K_1 patterns were performed after expressing an individual's regional parameters relative to that of the frontal cortex and on the specific *DV*, as defined above, with the use of the frontal cortex to estimate the nonsaturable total *DV* components. A significance threshold of $p < 0.05$ was employed throughout.

The possibility of age-related changes in K_1 or *DV* was further examined by linear regression analyses of parametric and relative parameter values. To facilitate comparisons with prior striatal aging data, apparent effects were expressed in linear (zero order) rates of change relative to extrapolated parameter values at birth (age, 0 years).

Results

Metabolites and Chromatography of [^{11}C]DTBZ

After systemic injection in the rat, [^{3}H]DTBZ and polar metabolites were identified in the liver and plasma, but only authentic DTBZ was recovered from the brain (Fig 1). In plasma, two groups of polar metabolites migrated at or near the origin on TLC. Liver chromatograms revealed similar bands of activity and another minor band of lower polarity. After isolation of the two predominant metabolite groups from liver, preliminary liquid chromatography studies revealed

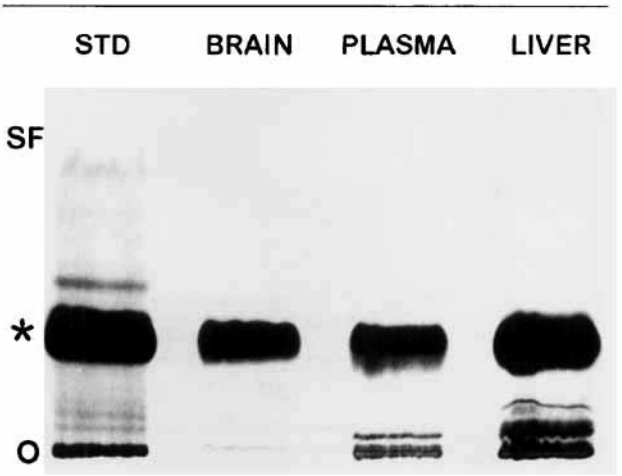

Fig 1. Autoradiographic visualization of [^{3}H]dihydrotetrabenazine ([^{3}H]DTBZ) and labeled metabolites from rat tissues. Samples of stock [^{3}H]DTBZ (STD) *and activities recovered from brain, plasma, and liver 15 minutes after injection were separated by thin-layer chromatography (TLC) and visualized by autoradiography. Subsequent liquid scintillation spectroscopy revealed more than 97% and 99% of total activity in the DTBZ standard and brain samples correspond to authentic DTBZ, respectively. Polar metabolites account for 14% and 7% of recovered activity from plasma and liver.* O = *chromatographic origin;* SF = *solvent front after TLC development;* * = *DTBZ.*

that they could be quantitatively removed from Sep-Pak C_{18} columns by elution with PBS/ethanol 65:35. This resulted in retention of more than 70% of authentic DTBZ on the column, which was subsequently recoverable in absolute ethanol. These chromatographic conditions were applied routinely in subsequent analyses of human plasma samples.

Human Plasma Activity after DTBZ Injection

After intravenous bolus injection of [^{11}C]DTBZ in human subjects, total plasma activity peaked rapidly and then declined by 20- to 50-fold within 5 minutes after injection (Fig 2A). Chromatography routinely revealed polar, labeled DTBZ metabolites after 5 minutes after injection that accounted for more than 50% of total plasma activity at the end of the 60-minute imaging period.

Normal Human Cerebral Distribution of DTBZ

Initial uptake of [^{11}C]DTBZ was relatively homogeneous and higher across gray matter than in white matter structures, consistent with the known pattern of cerebral blood flow. Within 3 to 5 minutes after injection, however, higher retention in the striatum was easily distinguished from other gray matter regions (Fig 2B). Between 5 and 7 minutes after injection, activity began to decline throughout the brain with slowest clearance from the caudate and putamen.

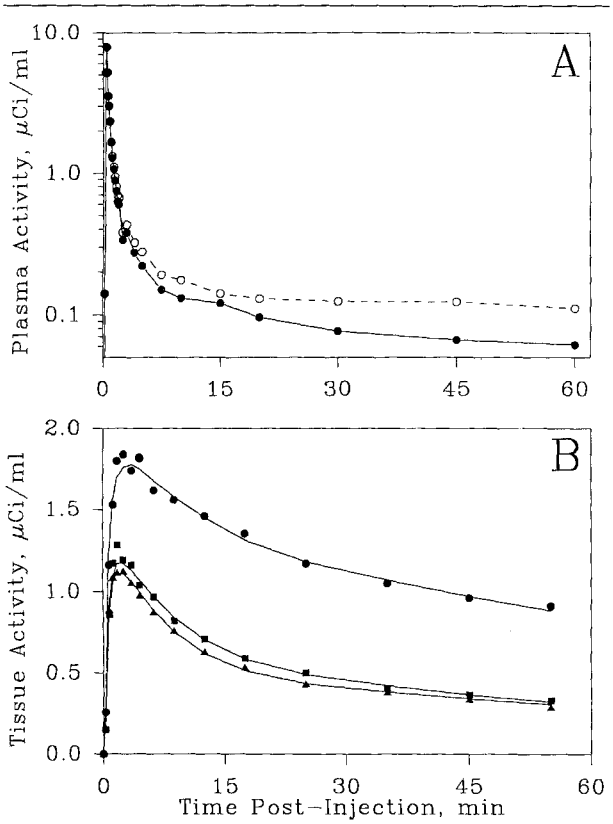

Fig 2. Time–activity curves after [^{11}C]dihydrotetrabenazine ([^{11}C]DTBZ) in a young normal subject. (A) Decay-corrected activities corresponding to total (open circles, dashed line) *and authentic DTBZ* (filled circles, solid line) *after rapid column chromatography are depicted. Note evidence for labeled metabolites after 5 minutes, accounting for more than 50% of total activity at 60 minutes. (B) Decay-corrected activities corresponding to regions-of-interest placed over the putamen* (circles), *thalamus* (squares), *and frontal cortex* (triangles) *are depicted together with the curves predicted by the model parameters determined in nonlinear least-squares analysis employing a three-compartment kinetic model (see Appendix). Note clear distinction of the putamen from other regions within 5 to 7.5 minutes after injection.*

Effect of Age on DTBZ Transport and Binding

Blood-to-brain transport of [^{11}C]DTBZ revealed similar values across the gray matter regions studied (Table 1, Fig 3), with average K_1 values between 0.29 and 0.34 ml of plasma/ml of brain/min in young normal subjects. The elderly controls demonstrated diminished K_1 in most of the regions studied. There were no group differences in the pattern of K_1 after expression relative to the frontal cortex, suggesting that the dominant aging effect on transport is a global reduction. Linear regression analyses revealed statistically significant declines in the striatal and cerebral cortical regions between 0.68% and 0.75% of extrapolated K_1 at birth per year, corresponding to approximately 35% declines between ages 20 and 70 years. Similar but statistically insignificant declining trends were found in the thalamus and cerebellum (reductions of 0.47% and 0.36% per year, respectively).

Binding of [^{11}C]DTBZ as reflected by the total tissue-to-plasma *DV* was regionally heterogeneous, displaying a 2.2-fold difference between putamen and cerebellum in young normal subjects (Table 2, see Fig 3). Total *DV* estimates were not significantly affected by age; however, there was a trend toward decline in striatal regions in the elderly controls. When specific *DV* was examined, a significant decline of 0.77% per year was revealed in the putamen (see Table 2; Fig 4).

Parkinson's Disease

Significant reductions in specific DTBZ *DV* were observed in the bilaterally averaged whole putaminal (−61%) and caudate nucleus (−43%) regions in PD compared with elderly controls (see Table 2). In contrast to DTBZ *DV*, K_1 values in the PD group tended to be higher than the elderly controls, achieving statistical significance in the cerebellum (see Table 1). When expressed relative to frontal cortex, the K_1 pattern in PD was virtually identical to that of the elderly controls and demonstrated no trend toward reduction in the striatal regions.

Regional analyses of individual PD patients' scans revealed reductions in whole-putaminal specific *DV*; *DV* was reduced below 2 SD of elderly control mean on at least one side in 5 of the 7 PD patients (Table 3). Considering the lowest specific putaminal *DV* in each elderly control and PD subject, there was no overlap between the two groups (elderly normal range, 0.41–0.95; PD range, 0.08–0.40). Inspection of pixel-by-pixel *DV* maps revealed clear reductions in putaminal *DV* in each PD subject, with the most severe loss in the posterior putamen (Fig 5). In each patient, the DTBZ *DV* was reduced to cerebral cortical levels in the posterior putamen on at least one side. In contrast, the entire putamen was well distinguished from adjacent cerebral cortex bilaterally in each elderly control. When reductions in PD patients' putamen *DV* measures were asymmetric, the most affected putamen was that contralateral to the most affected limbs.

Discussion

Measurement of VMAT2 with [^{11}C]DTBZ

The present work describes development and initial clinical research application of [^{11}C]DTBZ for nigrostriatal nerve terminal integrity measurement. The VMAT2 marker, targeted by DTBZ, has been shown previously to possess important characteristics related to its potential utility in neurodegenerative diseases. In the central nervous system, VMAT2 is expressed exclusively by monoaminergic neurons, including those utilizing dopamine, serotonin, norepinephrine, or hista-

Table 1. Plasma-to-Brain [^{11}C]DTBZ Transport[a]

	Frontal Cortex	Caudate	Putamen	Thalamus	Cerebellum
Parametric K_1					
Young normal	0.31 ± 0.07[b]	0.31 ± 0.09[b]	0.34 ± 0.10[b]	0.34 ± 0.06	0.29 ± 0.05
Middle-aged normal	0.34 ± 0.06[b]	0.35 ± 0.06[b]	0.38 ± 0.07[b]	0.42 ± 0.11[b]	0.35 ± 0.06[b]
Elderly normal	0.21 ± 0.07	0.20 ± 0.07	0.22 ± 0.08	0.26 ± 0.09	0.20 ± 0.07
Parkinson's disease	0.27 ± 0.04	0.27 ± 0.06	0.30 ± 0.06	0.34 ± 0.06	0.29 ± 0.05[b]
K_1 relative to frontal cortex					
Young normal	—	1.00 ± 0.17	1.09 ± 0.16	1.11 ± 0.14	0.93 ± 0.08
Middle-aged normal	—	1.03 ± 0.04	1.11 ± 0.02	1.23 ± 0.12	1.03 ± 0.04
Elderly normal	—	0.99 ± 0.15	1.07 ± 0.16	1.26 ± 0.04	0.99 ± 0.16
Parkinson's disease	—	1.00 ± 0.10	1.08 ± 0.11	1.23 ± 0.10	1.07 ± 0.12

[a]Values represent the mean ± SD of parametric K_1 estimates (ml of plasma/ml of brain/min) from three-compartment regional analyses, or K_1 expressed relative to that of frontal cortex, from 6 young, 3 middle-aged, and 6 elderly normal controls and 7 Parkinson's disease patients.
[b]Significant difference from elderly normal after one-way (within-region) analysis of variance at the $p < 0.05$ level by Student's t test.

DTBZ = dihydrotetrabenazine.

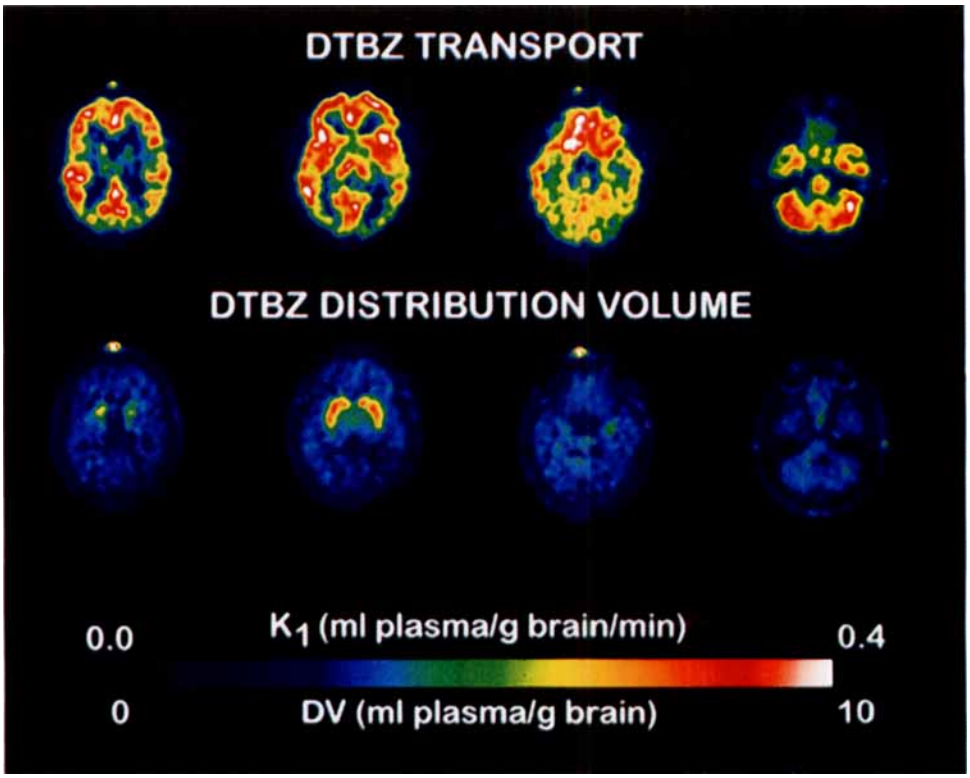

Fig 3. Parametric images of dihydrotetrabenazine (DTBZ) transport (K_1) and total distribution volume (DV) *from a representative young normal subject. DTBZ* K_1 *(top row) and total* DV *(bottom row) from a two-compartment, pixel-by-pixel estimation (see Appendix) are shown in five transaxial slices from supraventricular (left column) to the posterior fossa (right column) levels. The bright spots on the scalp at the top of images in columns 1 and 3 are due to the labeled fiducial markers used for dynamic image realignment.*

Table 2. [^{11}C]DTBZ Distribution Volume[a]

	Frontal Cortex	Caudate	Putamen	Thalamus	Cerebellum
Total *DV*					
Young normal	3.7 ± 0.6	7.4 ± 2.5	8.2 ± 2.8	3.9 ± 0.6	3.7 ± 0.8
Middle-aged normal	4.3 ± 0.5	7.9 ± 1.0	8.3 ± 1.2	4.6 ± 0.5	4.3 ± 0.8
Elderly normal	4.0 ± 0.8	7.0 ± 1.5	6.8 ± 1.4	4.3 ± 1.0	3.7 ± 0.8
Parkinson's disease	4.0 ± 0.9	5.6 ± 1.3	5.1 ± 1.2[b]	3.9 ± 0.9	4.1 ± 1.0
Specific *DV*					
Young normal	—	0.97 ± 0.38	1.18 ± 0.45[b]	0.05 ± 0.04	−0.02 ± 0.07
Middle-aged normal	—	0.84 ± 0.12	0.95 ± 0.18	0.07 ± 0.02	0.00 ± 0.12
Elderly normal	—	0.76 ± 0.18	0.70 ± 0.19	0.06 ± 0.06	−0.06 ± 0.13
Parkinson's disease	—	0.43 ± 0.26[b]	0.27 ± 0.11[c]	−0.02 ± 0.04	0.01 ± 0.07

[a]Values represent the mean ± SD of parametric total *DV* estimates (ml of plasma/ml of brain) from three-compartment regional analyses, or specific *DV* with the use of frontal cortex to estimate the nonsaturable *DV* component.
[b]Significant difference from elderly normal after one-way (within-region) analysis of variance at the $p < 0.05$ level by Student's t test.
[c]Significant difference from elderly normal at the $p < 0.001$ level by Student's t test.

DTBZ = dihydrotetrabenazine; *DV* = distribution volume.

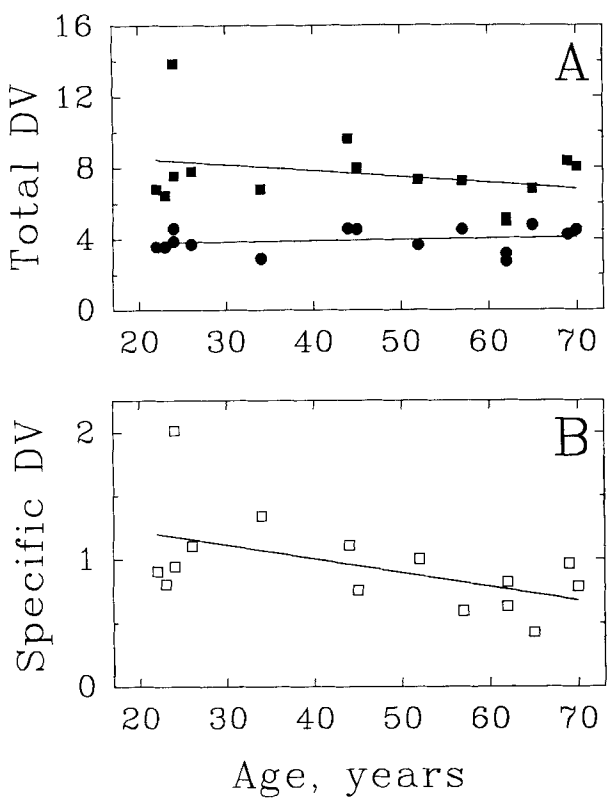

Fig 4. Effect of normal aging on dihydrotetrabenazine (DTBZ) total distribution volume (DV). *(A) Total tissue* DV *(ml of plasma/ml of tissue) determined regionally with a three-compartment kinetic model (see Appendix) is depicted in the putamen* (filled squares, DV = *9.204 − 0.034 [Age];* r = *0.303,* p = *0.272) and in the frontal cortex* (filled circles, DV = *3.658 + 0.006 [Age];* r = *0.169,* p = *0.547). (B) Specific DTBZ* DV *in the putamen. A significant decline with aging is identified:* DV = *1.432 − 0.011 [Age];* r = *0.531,* p = *0.042.*

mine [27, 29]. In both the rat [19] and human [30] striatum, however, the relative abundance of dopamine terminals of the nigrostriatal system renders more than 95% of the VMAT2 signal specific to this projection. Lesion studies in experimental animals verify that there is a linear correlation between substantia nigra pars compacta neuron integrity and ipsilateral striatal VMAT2 binding density [19], although residual binding to nondopaminergic VMAT2 sites may dominate after profound nigrostriatal reductions. Furthermore, there is evidence that VMAT2 does not undergo compensatory up- or down-regulation under conditions that alter the synthesis or release of dopamine or that alter the occupancy of dopamine receptors in experimental animals [17]. Thus, striatal DTBZ binding is a sensitive and specific marker of nigrostriatal dopaminergic innervation. A practical advantage of in vivo VMAT2 assys is that measures can be performed without discontinuation of symptomatic DOPA-mimetic therapy, as indicated by recent studies in experimental animals [31]. A relative disadvantage of VMAT2 as an imaging target may be its wide expression in the brain, precluding the use of a reference region entirely devoid of specific binding. As indicated in the present studies, however, this may not limit use of reference regions such as the cerebral cortex or cerebellum for estimation of specific striatal binding, since the latter regions have very high relative VMAT2 levels. Nevertheless, experimental designs must guard against changes in the chosen reference region, as may be assessed by the parametric (relative to blood) total DTBZ *DV.*

In contrast to the relationship between nigrostriatal terminal numbers and VMAT2 sites, other presynaptic dopaminergic imaging markers identify aspects that are now appreciated to undergo compensatory regulation. Uptake of the earliest in vivo imaging marker of striatal

Table 3. Specific Putamen [^{11}C]DTBZ Distribution Volumes in Individual Parkinson's Disease Patients

Patient No.	Age (yr)/ Sex	Duration (yr)/ Stage[a]	Medications[b]	Putamen/Cortex [^{11}C]DTBZ *DV*[c]	
				Left	Right
1	79/F	3/I	Levodopa, 300 mg	0.37	0.38
2	57/F	5/II	Levodopa, 480 mg Amantadine, 300 mg	0.15	0.50
3	64/M	2/II	Levodopa, 750 mg	0.26	0.31
4	70/M	3/II	Levodopa, 300 mg Deprenyl, 10 mg	0.40	0.43
5	60/M	10/III	Levodopa, 840 mg Deprenyl, 5 mg	0.08	0.17
6	67/M	4/III	Levodopa, 680 mg Deprenyl, 10 mg	0.24	0.16
7	70/M	6/III	Levodopa, 740 mg Deprenyl, 5 mg	0.15	0.15

[a]Duration of PD symptoms and disease severity as assessed on the scale of Hoehn and Yahr [21] at the time of PET scanning.
[b]Total daily doses of medications at the time of PET scanning. Continuous release levodopa (Sinemet CR) doses were scaled by 0.80 to reflect incomplete bioavailability of this preparation.
[c]Individual, whole putamen, specific DTBZ *DV*. Values for elderly normal subjects average 0.70 ± 0.19 (range, 0.41–0.98). Patient values less than 0.32 are 2 SD below normal and are considered significantly reduced.

DTBZ = dihydrotetrabenazine; *DV* = distribution volume; PD = Parkinson's disease; PET = positron emission tomography.

dopamine terminals [^{18}F]FDOPA, is predominantly related to the activity of DOPA decarboxylase (DDC) [32]. Although regulation of the rate-limiting dopamine synthetic enzyme tyrosine hydroxylase is well known, only recently has evidence for regulation of subsequent DOPA decarboxylation been sought. The decarboxylation rate has now been shown to be regulated by negative feedback from presynaptic dopamine D2 autoreceptors [33–36]. Thus, diseases or treatments that reduce synaptic dopamine levels will maximally activate DDC, resulting in compensatory increase in [^{18}F]FDOPA accrual within surviving terminals.

Several cocaine-analogue ligands have been introduced recently as markers of dopamine nerve terminals by virtue of their binding to the presynaptic, plasma membrane dopamine reuptake site (the dopamine transporter; DAT). Radioligands including the positron-emitting [^{11}C]WIN 35,428 [14] and the single photon–emitting [^{123}I]β-CIT [15] have successfully imaged striatal dopamine terminals in human brain. However, as in the instance of DDC, the DAT binding site density is subject to regulation by some drug treatments that alter synaptic dopamine levels and turnover, including classes of agents used in the symptomatic treatment of PD [17, 37–40].

Because of the merits of VMAT2 as a nigrostriatal marker, we have pursued several candidate radioligands for its determination in vivo with PET. Our initial selection, [^{11}C]tetrabenazine ([^{11}C]TBZ), permitted visualization of the human striatum; however, quantification of the signal could not be achieved due to the presence and abundance of pharmacologically active, labeled metabolites, including [^{11}C]DTBZ [41]. We next studied the metabolically directed TBZ analogue 2-*O*-methyldihydrotetrabenazine (methoxytetrabenazine; MTBZ), radiolabeled in a position chosen to slow its rate of metabolism and to yield unlabeled metabolites after *O*-demethylation. We achieved successful quantification of human VMAT2 with [^{11}C]MTBZ but discovered the presence of a minor labeled metabolite in rodent brain [16]. Our present studies with the TBZ metabolite DTBZ are even more encouraging. We find no evidence for labeled metabolites of DTBZ in brain and detect only polar metabolites in blood. In addition, the synthesis of [^{11}C]DTBZ is accomplished with higher yield and reliability than those of [^{11}C]MTBZ. Finally, we have recently demonstrated both in vitro [23] and in vivo [42] that the isomers of the racemic DTBZ employed here display marked differences in VMAT2 binding affinity. After chiral chromatographic resolution of the desmethyl precursor, the active isomer (+)-[^{11}C]DTBZ has now been prepared and demonstrates almost twofold higher relative human striatal accumulation than in the present studies [42]. Thus, future studies employing (+)-DTBZ should be even more sensitive to changes in VMAT2 expression.

The Nigrostriatal System in Aging

The present results in normal subjects indicate a significant age-associated decline in VMAT2 in the putamen. Regression analysis suggests loss of 0.77% per year of extrapolated specific DTBZ DV at birth. This

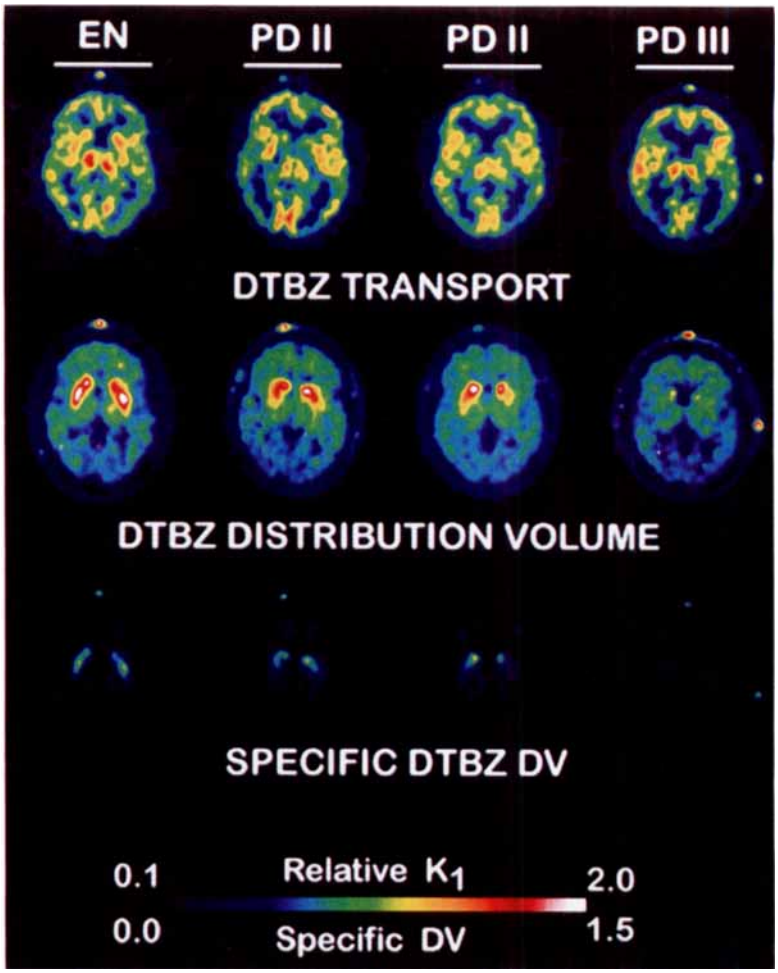

Fig 5. Parametric [^{11}C]dihydrotetrabenazine [^{11}C]DTBZ) images in Parkinson's disease (PD). Pixel-by-pixel maps of DTBZ transport and distribution volume (DV), *estimated from a simplified two-compartment model (see Appendix), are depicted in columns at a midstriatal level from representative control and PD subjects. [^{11}C]DTBZ transport (top row), total* DV *(middle row), and specific* DV *(bottom row) are displayed for each subject. Note substantial* DV *reductions in the posterior striata of all PD patients and virtual absence of specific* DV *in the most affected patient (right column).* EN = *elderly normal;* PD II = *Hoehn and Yahr [21] stage II PD;* PD III = *Hoehn and Yahr stage III PD.*

estimate is in good agreement with human postmorten studies on the loss of dopaminergic neurons from the substantia nigra pars compacta, suggesting 0.5 to 0.7% per year reduction [43, 44]. Postmortem assay of human striatal VMAT2 binding indicates a comparable age-associated loss of 0.74% per year [45]. Other laboratories have reported age-associated reductions in striatal DAT binding, both in vitro [46, 47] and in vivo, the latter assessed by PET with the use of [^{11}C]cocaine [48] or by single-photon emission computed tomography with the use of [^{123}I]β-CIT [15]. Estimated DAT changes are comparable with those indicated on our PET VMAT2 data, and range from 0.3 to 0.95% per year reductions.

In contrast to observed reductions in nigral neurons, VMAT2, and DAT, PET estimates of nigrostriatal innervation on the basis of [^{18}F]FDOPA uptake have revealed equivocal, conflicting evidence for change with advancing age. Two studies report age-associated declines of striatal FDOPA uptake between 0.3% and 0.7% per year [49, 50]. However, two additional reports from other laboratories fail to confirm these decreases, indicating unchanged [51] or slightly increased [52] striatal FDOPA uptake between 27 and 77 years of age. In agreement with these latter negative findings, Kish and co-workers [53] have recently examined DDC protein concentration in vitro. They report mild reduction in the caudate nucleus and no significant de-

cline in the putamen between ages 17 and 103 years, suggesting relatively increased expression of DDC per nerve terminal in aging.

Parkinson's Disease

Results of the present studies are encouraging regarding the use of [^{11}C]DTBZ to map and quantify the nigrostriatal terminal changes in PD. In agreement with postmortem VMAT2 binding assays [45, 54], we identified near-complete loss of specific DTBZ binding in the posterior putamen of each PD patient. We found no overlap of whole putamen–averaged DTBZ *DV* versus elderly controls, with significant individual putaminal reductions observed in 5 of 7 patients. Reductions of whole putamen, specific, DTBZ *DV* on the most severely affected sides of our PD patients averaged 68% (range, 43–89%). These changes are in good agreement with postmortem observations, suggesting 70–80% losses of striatal dopamine [2, 55] or of nigral neurons [44] are present when symptoms of PD are initially expressed.

In addition to other neurochemical markers of nigrostriatal injury, DAT binding is reduced by 90 to 95% in postmortem PD putamen [56–58]. In vivo DAT imaging studies have clearly demonstrated these reductions in PD [13, 14, 59]. DAT losses are correlated with the stage and severity of PD [59]; however, use of DAT binding to investigate possible disease-modifying aspects of therapy may not be possible due to its regulation as discussed previously.

Estimates of DDC with [^{18}F]FDOPA suggest more modest nigrostriatal losses than do our VMAT2 results. FDOPA K_i values often exceed 50% of control putaminal values in mild PD, and separation of PD from normal without overlap requires contrast between maximal caudate nucleus and minimal putamen K_i [60]. It may be speculated that the relative preservation of FDOPA K_i in PD striatum may result from up-regulation of DDC. This may arise chronically in association with accelerated dopamine turnover after partial destruction of the nigrostriatal pathway [61, 62] and also acutely during the obligatory discontinuation of levodopa therapy for FDOPA scanning [63]. In these instances, diminished synaptic dopamine levels may result in reduced occupancy of presynaptic D2 dopamine autoreceptors, leading to increased catalytic activity of DDC.

Summary

The present studies indicate the feasibility of imaging and quantification of VMAT2 sites in the human striatum with [^{11}C]DTBZ and PET. Lesions of the nigrostriatal pathway in PD and normal age-associated changes are demonstrated readily, without overlap of elderly normal and PD binding indices in the putamen. Combined with basic neurobiological evidence that VMAT2 binding site density is not subject to medication-induced or lesion-compensatory regulation, [^{11}C]DTBZ is well suited to future studies of PD progression and to the investigation of possible disease-modifying aspects of its treatment.

These studies were supported by grants to the investigators from the US Department of Energy and from the National Institutes of Health, designated DE-FG02-87ER60561 and P01 NS-15655, respectively. R.L.A. was supported by the GRECC at the Ann Arbor Veteran's Administration Medical Center.

Appendix

Modeling of DTBZ Distribution

A compartmental model incorporating intravascular tracer and free, nonspecifically bound and specifically bound tissue tracer pools (Fig 6) was employed for DTBZ *DV* estimation in the present studies. The model was simplified initially by combination of the nonspecific binding and free ligand pools, resulting in five parameters (blood volume and four intercompartmental exchange rates) to be estimated. The *DV* defined from the three-compartment, four-rate parameter model is as follows:

$$DV = K_1 (1 + k_3'/k_4)/k_2' \quad [1]$$

where K_1 is the blood-to-brain transport rate, k_2' represents brain-to-blood ligand transport, and k_3' represents binding to and k_4 represents dissociation from specific VMAT2 tissue sites. The $'$ designations in the notations k_2' and k_3' denote that they are apparent rates arising from combination of the tissue pools describing free and nonspecifically bound tracer. Kinetic regional estimates of *DV* were made by nonlinear, least-squares analyses [64] of tissue and arterial blood time–activity curves, as follows:

$$\mathrm{PET}(t) = C_T(t)(1 - BV) + C_A(t)BV \quad [2]$$

$$C_T(t) = \{K_1[k_3' + k_4 - X_1)e^{-X1t} + (X_2 - k_3' - k_4)e^{-X2t}]/(X_2 - X_1)\} * C_A(t) \quad [3]$$

where

$$X_1 = \{(k_2' + k_3' + k_4) - [(k_2' + k_3' + k_4)^2 - 4k_2'k_4]^{1/2}\}/2 \quad [4]$$

$$X_2 = \{(k_2' + k_3' + k_4) + [(k_2' + k_3' + k_4)^2 - 4k_2'k_4]^{1/2}\}/2 \quad [5]$$

PET (t) is the PET-determined tracer activity at time t, C_T and C_A are tracer concentrations in tissue and arterial blood, BV is the fractional tissue blood volume,

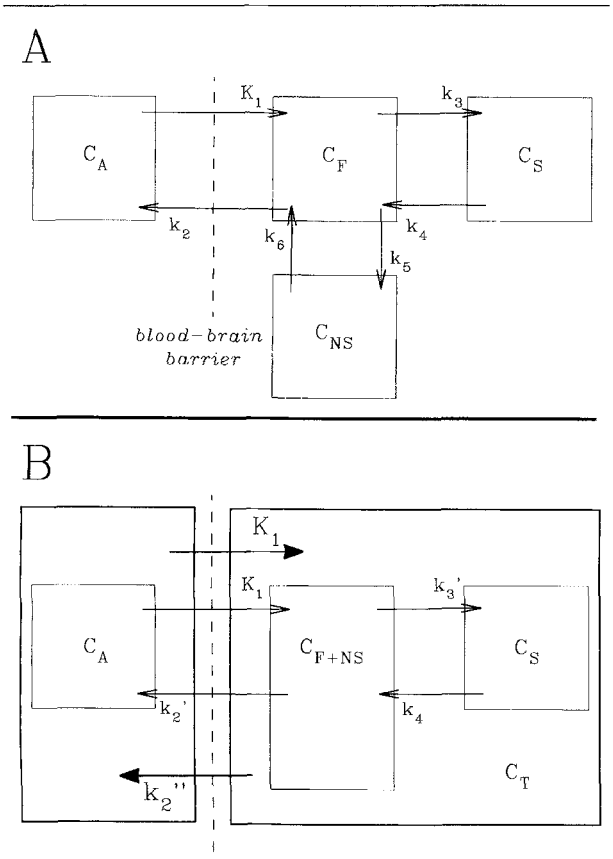

Fig 6. Physiologic compartmental model describing the distribution of dihydrotetrabenazine (DTBZ) in brain. (A) The most comprehensive model configuration includes arterial plasma tracer (C_A) *as well as individual representations of free tracer* (C_F), *nonspecific binding* (C_{NS}), *and specific binding* (C_S) *in tissue. Movement of tracer between compartments is governed by exchange rate constants designated* K_1 *and* k_2 *through* k_6. *The forward ligand-receptor binding rate constant in the model,* k_3, *is equivalent to the product* k_{on} R, *and the dissociation rate* k_4 *denotes* k_{off}, *where the available receptor concentration is denoted by* R *and the equilibrium binding affinity constant* $K_d = k_{on}/k_{off}$. *(B) Two model simplifications employed in the present analyses are depicted. The three-compartment configuration* (inner boxes, thin arrows) *assumes rapid equilibration of free and nonspecifically bound tracer in tissue, resulting in a new combined tissue pool* (C_{F+NS}) *and modified rate parameters* k_3' *and* k_2', *leading from it to the specifically bound and plasma tracer compartments, respectively. The modified rate parameters reflect underestimation of the actual binding and tissue-to-blood clearance rates due to the lack of correction for nonspecific binding in this configuration. The two-compartment model configuration* (outer boxes, thick arrows) *was employed for pixel-by-pixel estimation of DTBZ binding. In this instance, all tissue tracer is assumed within a single kinetic compartment, resulting in reduction to two-rate parameters* K_1 *and* k_2''. *The tissue-to-blood distribution volume* (DV) *is given by* K_1/k_2''.

and * represents the operation of convolution. In the fitting procedure, all parameters were constrained to positive values, and the value of k_4 was constrained to be greater than 0.02/min, since the 60-minute period of PET observation does not permit accurate determination of slower dissociation rates.

A further simplified two-compartment model, combining all tissue tracer activities into a single kinetic compartment (see Fig 6), was also used for calculation of pixel-by-pixel estimates of K_1 and DV by a rapid, weighted integral, lookup table approach [65] where

$$C_T(t) = K_1 e^{-k_2''} * C_A(t) \quad [6]$$

and

$$DV = K_1/k_2'' \quad [7]$$

The " in the designation of apparent rate constant k_2'' reflects its derivation from combining all three tissue compartments.

Our initial kinetic compartmental analyses of racemic [^{11}C]DTBZ in normal subjects indicate that the specific binding to and dissociation from VMAT2 sites in the striatum are sufficiently rapid that the binding parameters k_3' and k_4 cannot be precisely determined in isolation, as reported also for the resolved (+)-DTBZ isomer [66]. The total tissue DV, estimated either from the three-compartment or the two-compartment models, reveals excellent correlation with the known distribution of VMAT2 sites. The two models lead to DV estimates that are linearly correlated with one another; however, the three-compartment configuration leads to a broader dynamic range of DV values and better distinguishes regions of high and low VMAT2 site density. Thus, in the present studies, group differences in DV are assessed with the three-compartment model, while the detailed distribution of DV in individual subjects is depicted on a pixel-by-pixel basis with the two-compartment simplification.

References

1. Hornykiewicz O. Dopamine (3-hydroxytyramine) and brain function. Pharmacol Rev 1966;18:925–965
2. Kish SJ, Shannak K, Hornykiewicz O. Uneven pattern of dopamine loss in the striatum of patients with idiopathic Parkinson's disease. N Engl J Med 1988;318:876–880
3. Daniel SE. The neuropathology and neurochemistry of multiple system atrophy. In: Bannister R, Mathias CJ, eds. Autonomic failure: a textbook of clinical disorders of the autonomic nervous system. 3rd ed. Oxford: Oxford University Press, 1992:564–585
4. Steele JC, Richardson JC, Olszewski J. Progressive supranuclear palsy. A heterogeneous degeneration involving the brainstem, basal ganglia, and cerebellum, with vertical gaze and pseudobulbar palsy, nuchal dystonia and dementia. Arch Neurol 1964;10:333–358
5. Tanner CM, Langston JW. Do environmental toxins cause

Parkinson's disease? A critical review. Neurology 1990;40(suppl 3):17–30
6. Rajput AH. Environmental causation of Parkinson's disease. Arch Neurol 1993;50:651–652
7. Jenner P, Schapira AHV, Marsden CD. New insights into the cause of Parkinson's disease. Neurology 1992;42:2241–2250
8. Fahn S, Cohen G. The oxidant stress hypothesis in Parkinson's disease: evidence supporting it. Ann Neurol 1992;32:804–812
9. Sian J, Dexter DT, Lees AJ, et al. Alterations in glutathione levels in Parkinson's disease and other neurodegenerative disorders affecting basal ganglia. Ann Neurol 1994;36:348–355
10. The Parkinson Study Group. Effects of tocopherol and deprenyl on the progression of disability in Parkinson's disease. N Engl J Med 1993;328:176–183
11. Przedborski S, Jackson-Lewis V, Muthane U, et al. Chronic levodopa administration alters cerebral mitochondrial respiratory chain activity. Ann Neurol 1993;34:715–723
12. Garnett ES, Firnau G, Nahmias C. Dopamine visualized in the basal ganglia of living man. Nature 1983;305:137–138
13. Leenders KL, Salmon EP, Tyrrell P, et al. The nigrostriatal dopaminergic system assessed in vivo by positron emission tomography in healthy volunteer subjects and patients with Parkinson's disease. Arch Neurol 1990;47:1290–1298
14. Frost JJ, Rosier AJ, Reich SG, et al. Positron emission tomographic imaging of the dopamine transporter with ^{11}C-WIN 35,428 reveals marked declines in mild Parkinson's disease. Ann Neurol 1993;34:423–431
15. van Dyck CH, Seibyl JP, Malison RT, et al. Age-related decline in striatal dopamine transporter binding with iodine-123-β-CIT SPECT. J Nucl Med 1995;36:1175–1181
16. Vander Borght TM, Kilbourn MR, Koeppe RA, et al. In vivo imaging of the brain vesicular monoamine transporter. J Nucl Med 1995;36:2252–2260
17. Vander Borght T, Kilbourn M, Desmond T, et al. The vesicular monoamine transporter is not regulated by dopaminergic drug treatments. Eur J Pharmacol 1996;294:577–583
18. Naudon L, Leroux-Nicollet I, Costentin J. Short-term treatments with haloperidol or bromocriptine do not alter the density of the monoamine vesicular transporter. Neurosci Lett 1994;173:1–4
19. Vander Borght TM, Sima AAF, Kilbourn MR, et al. [^{3}H]Methoxytetrabenazine: a high specific activity ligand for estimating monoaminergic neuronal integrity. Neuroscience 1995;68:955–962
20. Gilman S, Frey KA, Koeppe RA, et al. Decreased striatal monoaminergic terminals in OPCA and MSA demonstrated with PET. Ann Neurol 1996 (In press)
21. Hoehn MM, Yahr, MD. Parkinsonism: onset, progression, and mortality. Neurology 1967;17:427–442
22. DaSilva JN, Kilbourn MR, Mangner TJ. Synthesis of [^{11}C]TBZ, a vesicular monoamine uptake inhibitor, for PET imaging studies. Appl Radiat Isot 1993;44:673–676
23. Kilbourn M, Lee L, Vander Borght T, et al. Binding of α-dihydrotetrabenazine to the vesicular monoamine transporter is stereospecific. Eur J Pharmacol 1995;278:249–252
24. Frey KA, Koeppe RA, Mulholland GK, et al. In vivo muscarinic cholinergic receptor imaging in human brain with [^{11}C]scopolamine and positron emission tomography. J Cereb Blood Flow Metab 1992;12:147–154
25. Frey KA, Holthoff VA, Koeppe RA, et al. Parametric in vivo imaging of benzodiazepine receptor distribution in human brain. Ann Neurol 1991;30:663–672
26. Koeppe RA, Frey KA, Mulholland GK, et al. [^{11}C]Tropanyl benzilate-binding to muscarinic cholinergic receptors: methodology and kinetic modeling alternatives. J Cereb Blood Flow Metab 1994;14:85–99
27. Scherman D, Raisman R, Ploska A, Agid Y. [^{3}H]Dihydrotetrabenazine, a new in vitro monoaminergic probe for human brain. J Neurochem 1988;50:1131–1136
28. Pearson SJ, Reynolds GP. Depletion of monoamine neurotransmitters by tetrabenazine in brain tissue in Huntington's disease. Neuropharmacology 1988;27:717–719
29. Erickson JD, Eiden LE. Functional identification and molecular cloning of a human brain vesicle monoamine transporter. J Neurochem 1993;61:2314–2317
30. Kish SJ, Robitaille Y, el-Awar M, et al. Striatal monoamine neurotransmitters and metabolites in dominantly inherited olivopontocerebellar atrophy. Neurology 1992;42:1573–1577
31. Kilbourn MR, Frey KA, Vander Borght T, Sherman PS. Effects of dopaminergic drug treatments on in vivo radioligand binding to brain monoamine transporters. Nucl Med Biol 1996 (In press)
32. Gjedde A, Reith J, Dyve S, et al. Dopa decarboxylase activity of the living human brain. Proc Natl Acad Sci USA 1991;88:2721–2725
33. Hadjiconstantinou M, Wemlinger TA, Sylvia CP, et al. Aromatic L-amino acid decarboxylase activity of mouse striatum is modulated via dopamine receptors. J Neurochem 1993;60:2175–2180
34. Young EA, Neff NH, Hadjiconstantinou M. Evidence for cyclic AMP-mediated increase of aromatic L-amino acid decarboxylase activity in the striatum and midbrain. J Neurochem 1993;60:2331–2333
35. Zhu M-Y, Jucrio AV, Paterson IA, Boulton AA. Regulation of striatal aromatic L-amino acid decarboxylase: effects of blockade or activation of dopamine receptors. Eur J Pharmacol 1993;238:157–164
36. Cumming P, Kuwabara H, Ase A, Gjedde A. Regulation of DOPA decarboxylase activity in brain of living rat. J Neurochem 1995;65:1381–1390
37. Weiner HL, Hashim A, Lajtha A, Sershen H. Chronic L-deprenyl-induced up-regulation of the dopamine uptake carrier. Eur J Pharmacol 1989;163:191–194
38. Ikegami H, Prasad C. Neuropeptide-dopamine interactions. V. Cyclo(his-pro) regulation of striatal dopamine transporter complex. Peptides 1990;11:145–148
39. Meiergerd SM, Hooks SM, Schenk JO. The striatal transporter for dopamine in the rat may be kinetically up-regulated following 3 weeks of withdrawal from cocaine self-administration. J Neurochem 1994;63:1277–1281
40. Wilson JM, Nobrega JN, Carroll ME, et al. Heterogeneous subregional binding patterns of ^{3}H-WIN 35,428 and ^{3}H-GBR 12,935 are differentially regulated by chronic cocaine self-administration. J Neurosci 1994;14:2966–2979
41. Kilbourn MR, DaSilva JN, Frey KA, et al. In vivo imaging of vesicular monoamine transporters in human brain using [^{11}C]tetrabenazine and positron emission tomography. J Neurochem 1993;60:2315–2318
42. Kilbourn MR, Lee LC, Jewett DM, et al. In vitro and in vivo binding of α-dihydrotetrabenazine to the vesicular monoamine transporter is stereospecific. J Cereb Blood Flow Metab 1995;15(suppl 1):S650 (Abstract)
43. McGeer PL, McGeer EG, Suzuki JS. Aging and extrapyramidal function. Arch Neurol 1977;34:33–35
44. Fearnley JM, Lees AJ. Ageing and Parkinson's disease: substantia nigra regional selectivity. Brain 1991;114:2283–2301
45. Scherman D, Desnos C, Darchen F, et al. Striatal dopamine deficiency in Parkinson's disease: role of aging. Ann Neurol 1989;26:551–557
46. Zelnik N, Angel I, Paul SM, Kleinman JE. Decreased density of human striatal dopamine uptake sites with age. Eur J Pharmacol 1986;126:175–176

47. De Keyser J, Ebinger G, Vauquelin G. Age-related changes in the human nigrostriatal dopaminergic system. Ann Neurol 1990;27:157–161
48. Volkow ND, Fowler JS, Wang GJ, et al. Decreased dopamine transporters with age in healthy human subjects. Ann Neurol 1994;36:237–239
49. Martin WRW, Palmer MR, Patlak CS, Calne DB. Nigrostriatal function in humans studied with positron emission tomography. Ann Neurol 1989;26:535–542
50. Cordes M, Snow BJ, Cooper S, et al. Age-dependent decline of nigrostriatal dopaminergic function: a positron emission tomographic study of grandparents and their grandchildren. Ann Neurol 1994;36:667–670
51. Sawle GV, Colebatch JG, Shah A, et al. Striatal function in normal aging: implications for Parkinson's disease. Ann Neurol 1990;28:799–804
52. Eidelberg D, Takikawa S, Dhawan V, et al. Striatal ^{18}F-DOPA uptake: absence of an aging effect. J Cereb Blood Flow Metab 1993;13:881–888
53. Kish SJ, Zhong XH, Hornykiewicz O, Haycock JW. Striatal 3,4-dihydroxyphenylalanine decarboxylase in aging; disparity between portmortem and positron emission tomography studies? Ann Neurol 1995;38:260–264
54. Lehéricy S, Brandel J-P, Hirsch EC, et al. Monoamine vesicular uptake sites in patients with Parkinson's disease and Alzheimer's disease, as measured by tritiated dihydrotetrabenazine autoradiography. Brain Res 1994;659:1–9
55. Bernheimer H, Birkmayer W, Hornykiewicz O, et al. Brain dopamine and the syndromes of Parkinson and Huntington. Clinical, morphological and neurochemical correlations. J Neurol Sci 1973;20:415–455
56. Niznik HB, Fogel EF, Fassos F, Seeman P. The dopamine transporter is absent in parkinsonian putamen and reduced in the caudate nucleus. J Neurochem 1991;56:192–198
57. Kaufman MJ, Madras BK. Severe depletion of cocaine recognition sites associated with the dopamine transporter in Parkinson's-diseased striatum. Synapse 1991;9:43–49
58. Chinaglia G, Alvarez FJ, Probst A, Palacios JM. Mesostriatal and mesolimbic dopamine uptake binding sites are reduced in Parkinson's disease and progressive supranuclear palsy: a quantitative autoradiographic study using [^{3}H]mazindol. Neuroscience 1992;49:317–327
59. Seibyl JP, Marek KL, Quinlan D, et al. Decreased single-photon emission computed tomographic [^{123}I]β-CIT striatal uptake correlates with symptom severity in Parkinson's disease. Ann Neurol 1995;38:589–598
60. Sawle GV, Playford ED, Burn DJ, et al. Separating Parkinson's disease from normality. Arch Neurol 1994;51:237–243
61. Hefti F, Melamed E, Wurtman RJ. Partial lesions of the dopaminergic nigrostriatal system in rat brain: biochemical characterization. Brain Res 1980;195:123–137
62. Zhong X-H, Haycock JW, Shannak K, et al. Striatal dihydrophenylalanine decarboxylase and tyrosine hydroxylase protein in idiopathic Parkinson's disease and dominantly inherited olivopontocerebellar atrophy. Mov Disord 1995;10:10–17
63. Gjedde A, Léger GC, Cumming P, et al. Striatal L-DOPA decarboxylase activity in Parkinson's disease in vivo: Implications for the regulation of dopamine synthesis. J Neurochem 1993;61:1538–1541
64. Marquardt DW. An algorithm for least squares estimation of nonlinear parameters. J Soc Indust Appl Math 1963;11:431–441
65. Alpert NM, Eriksson L, Chang JY, et al. Strategy for the measurement of regional cerebral blood flow using short-lived tracers and emission tomography. J Cereb Blood Flow Metab 1984;4:28–34
66. Koeppe RA, Frey KA, Vander Borght TM, et al. Kinetic evaluation of [^{11}C]dihydrotetrabenazine by dynamic PET: measurement of the vesicular monoamine transporter. J Cereb Blood Flow Metab 1996 (In press)